Impact of Representative Elemental Volume on Steady-State and Unsteady-State Relative Permeability

Guangyuan Sun*[1], *Andrew* Fager[1], *Bernd* Crouse[1], Christian Lange[2]

[1]Dassault Systèmes, USA
[2]Dassault Systèmes, Germany

Abstract. The comparison between steady-state relative permeability (SSRP) and unsteady-state relative permeability (USRP) is essential for accurately characterizing fluid flow in porous media. Under conditions dominated by capillary forces and a low capillary number, SSRP and USRP are generally expected to align closely, as both methods are governed by similar physical mechanisms. However, this agreement is contingent upon the sample being a Representative Elemental Volume (REV), which ensures that the sample captures the statistical homogeneity and relevant structural features of the porous medium. In this study, a multiphase lattice Boltzmann model (LBM) is employed to numerically measure both SSRP and USRP in the sample of Berea sandstone and carbonate as well as heterogeneous samples with rich clay content and fracture. A screening process to determine sample REV is introduced for quality check. Our results suggest that, when the samples do not represent an REV, the match between SSRP and USRP deteriorates due to scale effects and heterogeneity. Steady-state measurements fail to account for dynamic changes in fluid displacement over time, which are captured by unsteady-state methods. These findings emphasize the importance of using REV-scale samples to ensure the validity and reliability of permeability measurements. The mismatch between SSRP and USRP in non-REV samples presents challenges in the interpretation of permeability data and may lead to inaccurate predictions of fluid flow behavior. In addition, it is observed that the screening process in this study is good indicator to evaluate sample representativeness.

1 Introduction

Understanding multiphase flow through porous media is fundamental to a wide range of subsurface applications, including enhanced oil recovery, carbon capture and storage, and groundwater hydrology. A key component of this understanding lies in the accurate determination of relative permeability curves, which describe the ability of each fluid phase to flow in the presence of others. Two primary experimental approaches—steady-state and unsteady-state methods—are used to measure relative permeability. While both methods aim to characterize the same physical properties, they differ significantly in their operational procedures and sensitivities to various flow conditions.

Steady-state relative permeability (SSRP) measurements involve simultaneously injecting immiscible fluids at controlled flow rates until equilibrium is reached, whereas unsteady-state relative permeability (USRP) typically involves displacing one fluid with another while monitoring transient pressure and saturation changes. In theory, under capillary-dominated regimes—typified by low capillary numbers and slow displacement—the two methods should yield similar results due to the dominance of capillary equilibrium in both cases [1,2]. However, deviations between SSRP and USRP are frequently reported in literature, often attributed to differences in sample size, heterogeneity, and the dynamic nature of fluid fronts in unsteady-state experiments [3,4].

A central concept in resolving such discrepancies is the Representative Elemental Volume (REV), defined as the smallest volume over which a measurement can be made that will yield a value representative of the whole [5]. If the sample volume does not satisfy the conditions for REV due to heterogeneity, fractures, or clay-rich regions, the resulting measurements may not reflect the intrinsic properties of the porous medium. This issue becomes particularly pronounced when comparing SSRP and USRP, as non-REV samples may emphasize local heterogeneities or scale-dependent effects, leading to inconsistencies between the two methods [6].

Recent advances in pore-scale modeling, such as the Lattice Boltzmann Method (LBM), provide a robust framework for simulating complex multiphase flow processes under controlled digital conditions. These simulations allow for direct comparison of SSRP and USRP across a variety of rock types and microstructures, enabling detailed analysis of the influence of REV on measurement consistency [7-13].

In this work, we employ a multiphase LBM approach to investigate the impact of sample representativeness on the agreement between SSRP and USRP in both

* Corresponding author: Guangyuan.SUN@3ds.com

homogeneous (Berea sandstone) and heterogeneous samples (rich in clay or fractured). By introducing a quantitative screening process for REV identification, we aim to highlight the role of scale and heterogeneity in relative permeability measurements and emphasize the necessity of REV-scale sampling for reliable fluid characterization.

2 Methodology

2.1 Screening process

The screening and assessment of Representative Elementary Volume begin with high-resolution image acquisition, typically using micro-CT or other image scanning, followed by image processing to segment pore and solid phases accurately. Screening procedure involves evaluating connected porosity, pore size distribution, and the coefficient of variation across increasing subvolume sizes to identify the scale at which these properties stabilize. This stabilization point indicates the REV, beyond which further volume increase does not significantly change the measured properties. Screening is crucial for ensuring that simulations or experimental results, particularly steady-state and unsteady-state relative permeability calculations, reflect intrinsic rock behavior rather than artifacts of insufficient sample size. Proper REV identification ensures that fluid flow predictions are representative and reliable. The screening procedure is summarized in Figure 1, and each step is detailed in the subsequent sections.

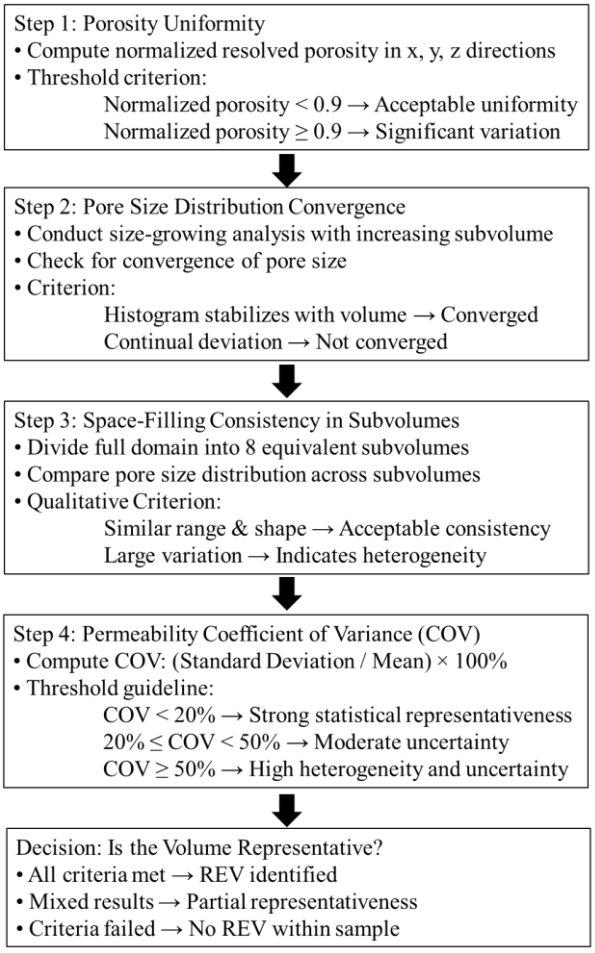

Fig. 1. Screening process of representative elementary volume.

2.1.1 Connected porosity uniformity

The evaluation of porosity variability in all three spatial directions is crucial for determining whether a given rock sample qualifies as a Representative Elemental Volume (REV). In heterogeneous porous media, local fluctuations in porosity can lead to significant variations in transport properties such as permeability and relative permeability, which may not be captured accurately if the sample is not representative of the larger system. A key indicator of sample representativeness is the uniformity of porosity across the sample volume. If porosity exhibits substantial variation especially along different directions, this often signals that the sample is too small or too heterogeneous to serve as an REV. To quantify this variability, a normalized porosity is defined as

$$\emptyset^* = \frac{\emptyset_{max} - \emptyset_{min}}{\emptyset_{mean}} \quad (1)$$

where $\emptyset_{max}$, $\emptyset_{min}$ and $\emptyset_{mean}$ are the maximum, minimum, and average porosities observed within the sample, respectively. This dimensionless quantity provides a standardized way to assess the degree of heterogeneity and has been widely used in digital rock physics and pore-scale modelling studies [14-16]. When the normalized porosity is high, it indicates significant structural variability, suggesting that the volume under consideration is insufficient to average out local heterogeneities, and therefore does not qualify as an REV. Incorporating such quantitative metrics is essential for robust sample screening and for ensuring that derived flow properties are reliable and upscalable. In this study, 0.9 is used as threshold criterion for normalized connected porosity.

2.1.2 Pore size distribution

Pore size distribution (PSD) is a critical microstructural property that influences fluid flow and transport in porous media and serves as a valuable criterion for evaluating the REV. The uniformity of PSD across a sample reflects the homogeneity of the pore network, and deviations may signal the presence of local heterogeneities that undermine the representativeness of the sample. To systematically assess this, subdomain analysis methods are employed to examine how PSD varies across space and scale. One such method is size-growing analysis, wherein the sample is progressively analyzed using overlapping, centered subdomains of increasing size but constant aspect ratio. As subdomain size increases,

convergence of PSDs suggests that the larger domain averages out local heterogeneities and approaches REV behavior. This method has been used extensively in digital rock physics to identify the scale at which rock properties stabilize [14].

Complementing this is space-filling analysis, in which the sample is partitioned into multiple, contiguous subdomains of equal size, typically eight, to preserve geometric balance. Each subdomain's PSD is evaluated independently, and the results are plotted as "rake curves" to visualize PSD variability with respect to location. When PSDs of all subdomains overlap closely, the rock is likely homogeneous, and the current sample may already qualify as an REV. Conversely, large discrepancies between curves suggest spatial heterogeneity, requiring larger or more representative sampling. This dual approach of size-growing and space-filling analysis offers a comprehensive view of spatial and scale-dependent variability and has proven effective in guiding REV identification in both experimental and computational studies [17,18].

2.1.3 Permeability coefficient of variation

The coefficient of variation (COV) analysis is a powerful and widely used method for evaluating the scale dependence of material properties in porous media and for determining the REV. It combines features from both space-filling and size-growing subdomain analysis techniques to provide a comprehensive assessment of spatial heterogeneity. In this approach, the analysis domain is divided into n^3 equally sized, contiguous subdomains, where n=2,3, … This setup ensures that the statistical variability of a given property, such as permeability, can be evaluated over multiple spatial configurations and scales. When the original domain is not perfectly cubic, an equivalent edge length is computed to enable consistent comparisons between subdomains of different shapes but equal volume. The goal is to determine whether the mean and variability of the property under investigation stabilize as the size of the subdomains increases, which is a key criterion for identifying an REV.

COV is defined as the ratio of the standard deviation to the mean of a random variable across a given set of subdomains. This dimensionless quantity characterizes relative variability and is particularly useful in geosciences and rock physics because it provides a normalized measure of uncertainty, independent of the absolute magnitude of the measured property. Statistically, COV can be interpreted as indicating the likelihood that a randomly selected subdomain will deviate significantly from the mean value. For each subdomain size (or equivalent edge length), the COV of the permeability estimator is computed. As the subdomain size increases, spatial heterogeneities become averaged out, and the standard deviation typically decreases relative to the mean, resulting in a lower COV. Therefore, a decreasing COV with increasing domain size suggests that the sample is approaching statistical homogeneity, and hence, an REV has been reached [14,17].

Importantly, COV analysis is not just a diagnostic tool but also a quantitative measure of uncertainty in the derived material properties. High COV values indicate large variability among subdomains and suggest that the domain size is insufficient for reliable upscaling of flow properties such as permeability and relative permeability. Conversely, when COV falls below a certain threshold (e.g., 20% or 50%), the property in question can be considered stable and representative of the medium as a whole. Studies across various rock types can use COV analysis to ensure that simulation domains are large enough to capture essential pore-scale features while minimizing computational cost. The use of COV as an REV criterion thus enables a rigorous and repeatable framework for assessing representativeness in porous media analysis. In this study, a permeability coefficient of variation (COV) below 20% is interpreted as indicative of strong statistical representativeness. COV values between 20% and 50% suggest a moderate level of uncertainty in the representativeness of the sample. When the COV exceeds 50%, it reflects pronounced heterogeneity and significant statistical uncertainty.

2.2 Numerical simulation procedure

All flow simulations in this study were conducted using DigitalROCK™, a digital rock physics platform that employs a multiphase lattice Boltzmann solver based on the Shan–Chen pseudopotential model [7]. This numerical method has been rigorously validated against benchmark studies and experimental data from real reservoir rock samples [8-13,19-20].

Two numerical protocols were employed to replicate steady-state and unsteady-state relative permeability measurements, reflecting standard laboratory coreflood methodologies. In both cases, periodic boundary conditions were applied along the primary flow direction, with no-flow conditions imposed on the transverse boundaries. Fluid properties, including the viscosity ratio and capillary number, were defined to match either laboratory test conditions or representative field scenarios.

2.2.1 Unsteady-State Simulation

Unsteady-state relative permeability simulations emulate coreflood experiments where water displaces oil from a porous medium. In this approach, water is continuously injected at the inlet boundary, while both oil and water are produced at the outlet. A thin buffer zone downstream of the outlet serves to separate the fluids and remove oil, ensuring that only water is recirculated back to the inlet. The simulation proceeds until the oil production rate drops to zero, indicating the completion of the displacement process. This methodology enables the determination of relative permeability by tracking the dynamic saturation and flow rates of each phase during the displacement.

2.2.2 Steady-State Simulation

Steady-state simulations are designed to evaluate relative permeability at fixed saturation conditions. The simulation sequence begins with a specified initial water saturation and progresses toward residual oil saturation. Fluid mixtures with increasing water-to-oil ratios are injected in steps, with each saturation state maintained until a steady-state flow regime is reached and defined by the convergence of phase flow rates. At each equilibrium point, the relative permeabilities of oil and water are calculated. This process is repeated incrementally, allowing for the construction of complete relative permeability curves. The steady-state simulations employed in this study implement an imbibition displacement protocol in which water is injected into an initially oil-saturated system. Flow is allowed to equilibrate at each saturation level before permeability measurements are taken, and the process is repeated until a residual water-saturated state is achieved and the water phase is nearly immobile.

2.2.3 Initial Conditions and Flow Regime

To establish initial fluid distributions for all simulations, a capillary-driven drainage process was used. The extended primary drainage method was applied, resulting in a water saturation of approximately 5–15% by volume, typically occupying the smallest pore throats. A uniform contact angle of 30° was assigned to all solid surfaces to represent a strongly water-wet condition. All simulations were performed under capillary-dominated flow conditions, with the capillary number (N_c) on the order of 10^{-5}. The capillary number is defined as:

$$N_c = \frac{q\mu}{\sigma} \tag{2}$$

where q is the Darcy velocity, μ is the viscosity of the invading fluid and σ is the interfacial tension between the two immiscible fluids. This flow regime ensures that capillary forces dominate over viscous forces, which is representative of typical conditions encountered in laboratory-scale relative permeability experiments and many subsurface reservoirs.

2.3 Rock sample

In this study, three rock samples with varying degrees of heterogeneity were selected to investigate the influence of pore structure and heterogeneity on flow behavior and representative elemental volume (REV) analysis. The samples include a homogeneous Berea sandstone and two heterogeneous rocks: a fractured sample and a clay-rich shale. Each sample was imaged using high-resolution techniques suitable for capturing the relevant pore structures and flow pathways. The imaging results were subsequently used to perform single-phase flow simulations to quantify absolute permeability and assess fluid transport characteristics.

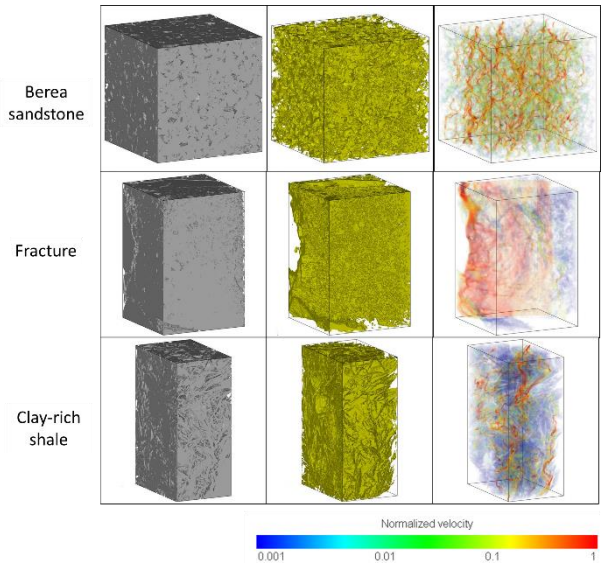

Fig. 2. 3D view of rock samples (left), pore space (middle) and velocity field (right).

The Berea sandstone sample represents a relatively homogeneous and isotropic porous medium, often used as a benchmark material in petrophysical studies. A cylindrical plug with a diameter of 5 mm and a length of 10 mm was scanned using micro-computed tomography (micro-CT) at a spatial resolution of 2.02 µm/voxel. This resolution enabled accurate reconstruction of the pore space, facilitating detailed visualization of the grain and void geometry. From the segmented images, the resolved porosity was calculated to be 15.7%. A single-phase flow simulation was conducted on the digital rock model, yielding an absolute permeability of 235 millidarcies (mD), which aligns well with established literature values for Berea sandstone. The uniform distribution of pores and lack of large-scale heterogeneities make this sample ideal for examining baseline flow behavior in homogeneous media.

To contrast with the Berea sample, a naturally fractured rock and a clay-rich shale were selected to capture the complexity of heterogeneous porous systems. The fractured sample was scanned using micro-CT imaging at a higher resolution of 1.5 µm/voxel to adequately resolve the fracture network and surrounding matrix. Although the resolved porosity was lower at 8.9%, the presence of interconnected fractures dramatically enhanced permeability, resulting in an absolute permeability of 725 mD as determined from the flow simulation. The third sample, a clay-rich shale, required even higher imaging resolution due to its nanoporous structure. This sample was imaged using focused ion beam scanning electron microscopy (FIB-SEM) at an ultra-fine resolution of 0.015 µm/voxel, allowing for the reconstruction of its intricate pore network. The resolved porosity was notably high at 31.8%; however, due to poor pore connectivity, the calculated absolute permeability was extremely low at 0.0047 mD. These results highlight the contrasting flow regimes present in different geological media. Figure 2 presents the 3D pore geometries and velocity field visualizations for each sample, illustrating the significant differences in flow

pathways and magnitudes governed by pore-scale heterogeneity.

3 Results and discussion

3.1 Berea sandstone

In this section, we present the results of the screening procedure applied to the Berea sandstone sample, followed by a comparative analysis of steady-state and unsteady-state relative permeability (SSRP and USRP, respectively). The primary objective is to identify an appropriate representative elementary volume (REV) and evaluate how REV influences the accuracy and consistency of multiphase flow measurements.

The screening procedure begins with the analysis of connected resolved porosity profiles along three directions (Figure 3). As shown in Table 1, the normalized resolved porosities are calculated as 0.46, 0.37, and 0.48 in the x-, y-, and z-directions, respectively. All values fall well below the REV threshold of 0.9, indicating a relatively uniform porosity distribution without significant directional variation or large-scale heterogeneity. This outcome aligns with the known homogeneous nature of Berea sandstone and suggests the absence of preferential flow paths or anisotropic porosity features at the scanned scale. However, it is important to recognize that porosity alone does not fully determine REV; spatial variation in other microstructural parameters such as pore size and connectivity must also be considered.

Subsequently, pore size distribution was assessed using a size-growing analysis, where convergence is used as an indicator of volumetric representativeness. Figure 4 illustrates that the distribution deviates noticeably at smaller sample volumes, stabilizing only once the volume exceeds 500^3 voxels. This convergence implies that key structural features, including both large and small pore bodies, are statistically represented within this volume. Figure 5 supports this through space-filling analysis, in which eight equivalent subvolumes demonstrate only minor variability in pore size distribution. The observed differences, although small, suggest that microstructural heterogeneity still exists locally and can influence fluid transport behavior, particularly in smaller samples. To quantify these effects, permeability coefficient of variation (COV) was calculated for the 300^3 and 500^3 voxel subsets. As shown in Figure 6, the COV values were 26.3% and 15.8%, respectively. This marked reduction in variability with increasing volume confirms that the 500^3 voxel subset is more statistically representative of the bulk sample and is thus selected as the REV. The smaller 300^3 voxel subset is retained for comparison to evaluate the sensitivity of multiphase flow results to sub-REV scale selection.

Multiphase flow simulations were then performed to compare SSRP and USRP behavior across these two volumes. Figure 7 presents the results for the non-REV 300^3 voxel subset, where a deviation between SSRP and USRP is observed. Notably, the oil relative permeability in USRP exceeds that of SSRP, indicating enhanced connectivity of the oil phase during unsteady-state displacement. This discrepancy arises from the dynamic nature of USRP, where the evolving front and capillary-driven redistribution of fluids can produce higher apparent mobility in the absence of full pore-filling equilibrium. Moreover, the physical validity of USRP results is limited prior to water breakthrough due to the absence of a continuous water phase spanning from inlet to outlet. As illustrated in Figure 8, this limitation is especially pronounced near the inlet, where end effects dominate. To minimize this artifact, the first 20% of the sample volume adjacent to the inlet was excluded from the analysis. Despite this correction, the small volume of the 300^3 voxel subset is insufficient to average out localized pore-scale effects, leading to inconsistencies between SSRP and USRP.

When the analysis is repeated on the REV-sized 500^3 voxel subset, the results demonstrate significant improvement in both consistency and reliability. As seen in Figures 7 and 8, SSRP and USRP curves show strong agreement, with similar trends across the entire saturation range. Furthermore, Figure 9 shows that the spatial profiles of residual water saturation at the end of simulation are well aligned between the two methods. This agreement confirms that the selected REV volume is sufficient to capture the full range of flow pathways, pore-scale interactions, and displacement mechanisms. The importance of REV is particularly evident in the context of USRP, where dynamic saturation fronts and local heterogeneities exert a strong influence on relative permeability curves. Without a representative volume, these effects introduce significant bias, leading to erroneous interpretation of flow characteristics.

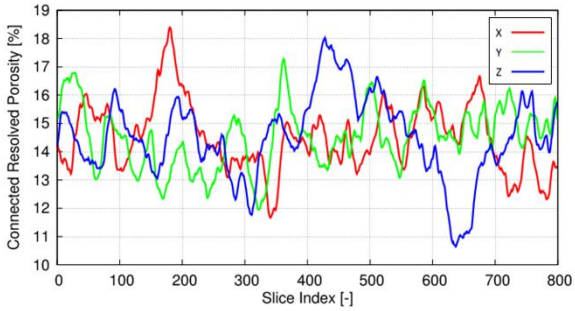

Fig. 3. Connected resolved porosity profiles of Berea sandstone.

Table 1. Normalized resolved porosity ($\emptyset^*$) of Berea sandstone.

X	Y	Z
0.46	0.37	0.48

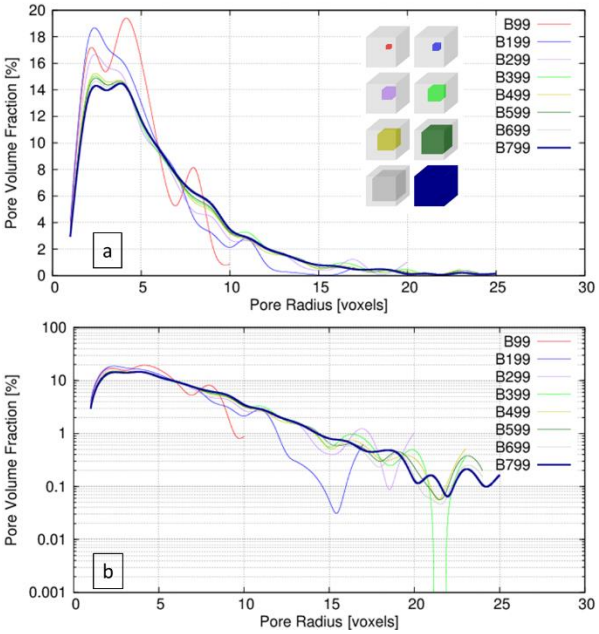

Fig. 4. Size growing analysis of pore size distribution of Berea sandstone in (a) linear scale and (b) logarithmic scale.

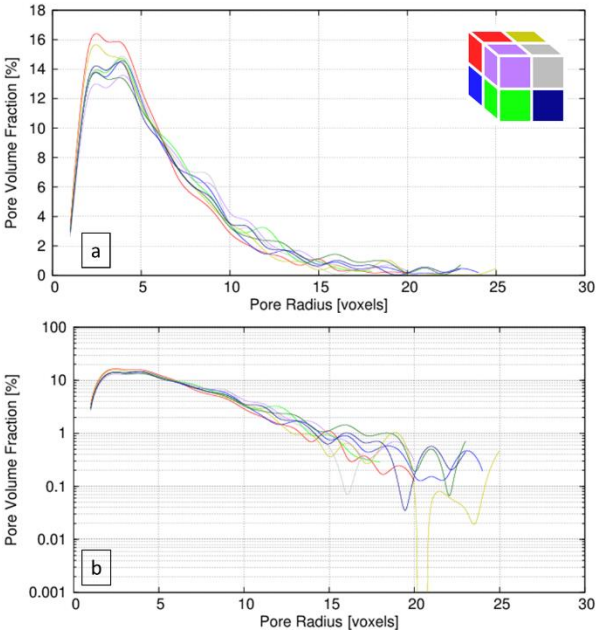

Fig. 5. Space filing analysis of pore size distribution of Berea sandstone in (a) linear scale and (b) logarithmic scale.

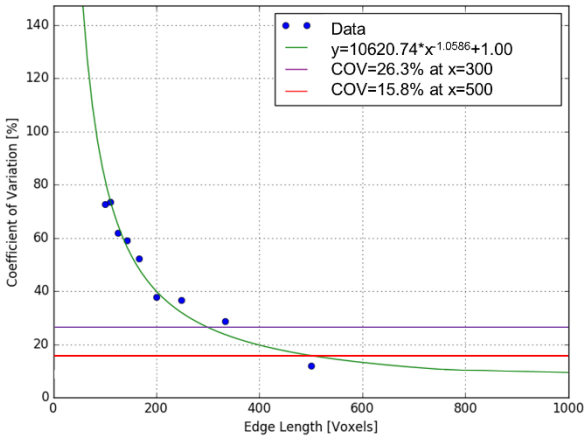

Fig. 6. Permeability coefficient of variance (COV) of Berea sandstone.

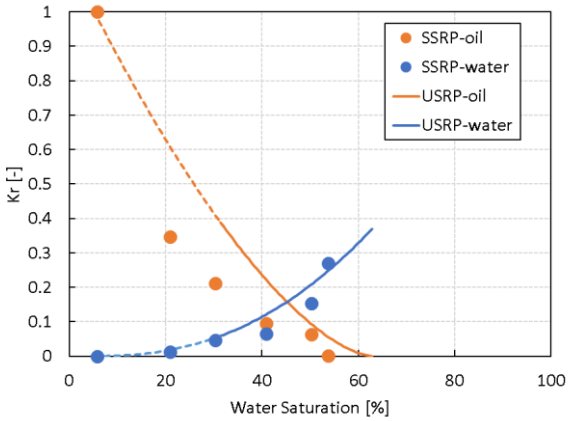

Fig. 7. Steady state relative permeability (SSRP) vs. unsteady state relative permeability (USRP) of 300^3 voxels subset of Berea sandstone. Dash line and solid line represents the measurements before and after water breakthrough, respectively.

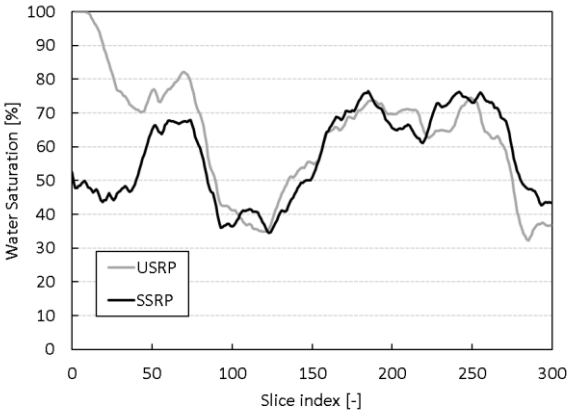

Fig. 8. Water saturation profile of 300^3 voxels subset of Berea sandstone at residual saturation of steady state relative permeability (SSRP) and unsteady state relative permeability (USRP).

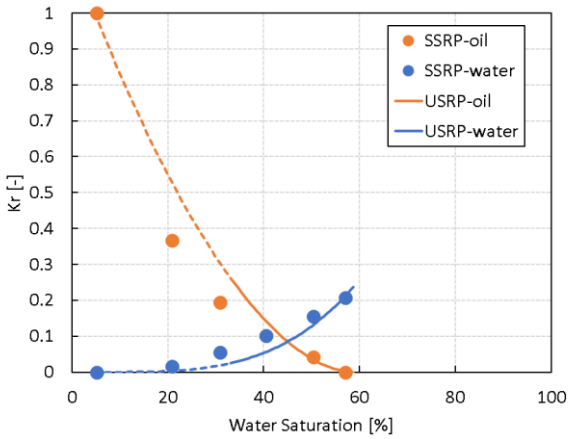

Fig. 8. Steady state relative permeability (SSRP) vs. unsteady state relative permeability (USRP) of 500^3 voxels subset of Berea sandstone. Dash line and solid line represents the measurements before and after water breakthrough, respectively.

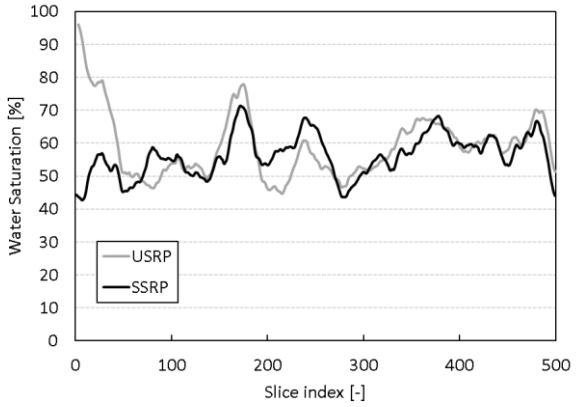

Fig. 9. Water saturation profile of 500^3 voxels subset of Berea sandstone at residual saturation of steady state relative permeability (SSRP) and unsteady state relative permeability (USRP).

3.2 Fracture sample

The fractured rock sample represents a highly heterogeneous medium, and the results of the screening procedure clearly reflect the complexity inherent to such systems. As shown in Figure 10, the connected resolved porosity profiles exhibit significant variation across all three principal directions. The normalized resolved porosities are calculated as 1.12, 2.11, and 1.17 in the x-, y-, and z-directions, respectively, each exceeding the REV threshold of 0.9. This high degree of directional variability reveals substantial heterogeneity in the porosity distribution, likely caused by the presence of dominant fractures intersecting the porous matrix. These values point to the absence of volumetric uniformity and indicate that the scanned sample cannot be assumed to be statistically homogeneous along any spatial axis. Such variability is typical of fractured systems, where large, discrete voids (fractures) coexist with fine-grained matrix pores, leading to anisotropic and discontinuous pore structures.

Further insight into the heterogeneity is obtained from the pore size distribution analysis. The pore size growing curves in Figure 11 show no clear convergence, even as the analyzed volume approaches the full extent of the scan. This persistent deviation indicates that larger representative volumes would still fail to capture a stable statistical distribution of pore sizes, a signature characteristic of structurally complex fractured media. Complementary to this, the space-filling analysis shown in Figure 12 further illustrates the spatial inconsistency of pore size distributions across the domain. Eight subvolumes, each extracted from the full scanned region, demonstrate pronounced differences in both the range and shape of the pore size histograms. This reinforces the conclusion that no subvolume within the scanned domain can be reliably considered as a representative sample of the entire structure. The permeability analysis supports these observations: as shown in Figure 13, the coefficient of variation (COV) of permeability across the entire volume reaches 75.4%, a value that underscores the statistical unreliability of the sample volume for deriving generalizable flow properties. High COV values are typically associated with fractured media, where permeability is dominated by a few large flow paths rather than the bulk pore network.

Given the lack of REV, the interpretation of multiphase flow behavior must be approached with caution. In Figure 14, SSRP and USRP results for the whole fractured sample are compared. The observed mismatch between the two methods is evident: SSRP yields higher water-phase relative permeability than USRP across the saturation range. This divergence suggests differing displacement dynamics in the two experimental approaches. In the SSRP method, water reaches a steady flow state where it preferentially invades and fills the largest, most connected pathways (typically fractures) leading to higher apparent mobility. In contrast, USRP involves a dynamic invasion process where capillary trapping, bypassing, and delayed water breakthrough are more pronounced due to complex pore-throat geometry and disconnected flow paths. This is particularly evident in the water saturation maps at residual conditions (Figure 15), where the final saturation profiles diverge significantly between SSRP and USRP. These differences imply that fluid pathways activated during unsteady-state displacement are not fully aligned with those engaged during steady-state flow, especially in a structure where connectivity is highly localized.

The screening procedure confirms that the fracture sample does not contain an identifiable REV within the scanned domain. The high variability in porosity, pore size distribution, and permeability all point to a system that defies the representativeness.

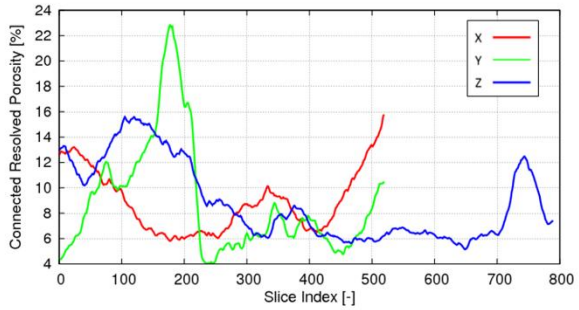

Fig. 10. Connected resolved porosity profiles of fracture sample.

Table 2. Normalized resolved porosity ($\emptyset^*$) of fracture sample.

X	Y	Z
1.12	2.11	1.17

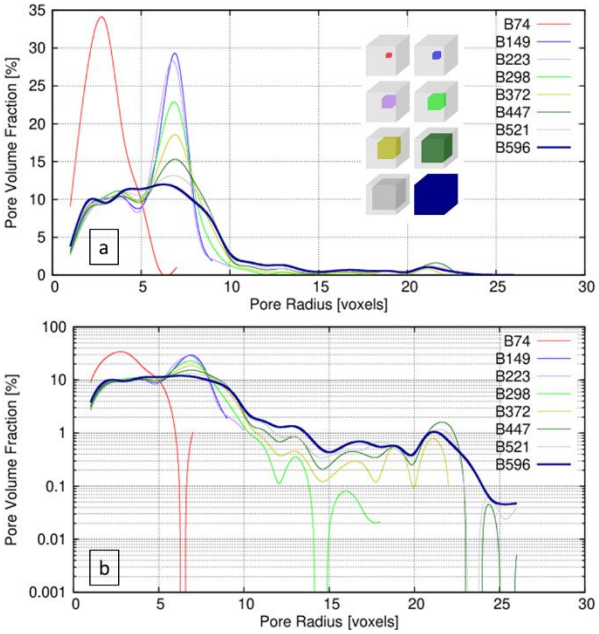

Fig. 11. Size growing analysis of pore size distribution of fracture sample in (a) linear scale and (b) logarithmic scale.

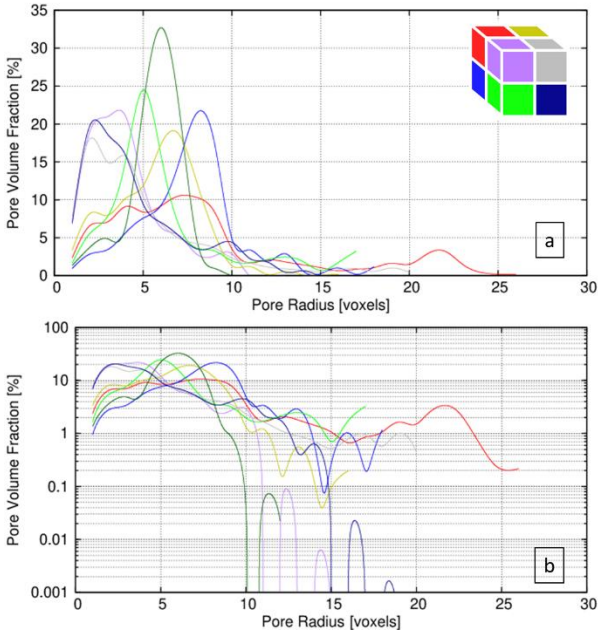

Fig. 12. Space filing analysis of pore size distribution of fracture sample in (a) linear scale and (b) logarithmic scale.

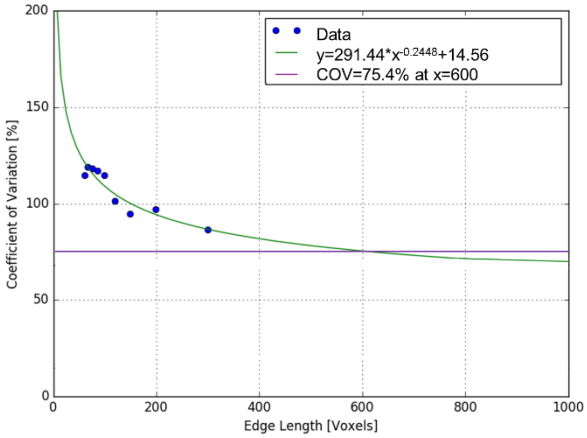

Fig. 13. Permeability coefficient of variance (COV) of fracture sample.

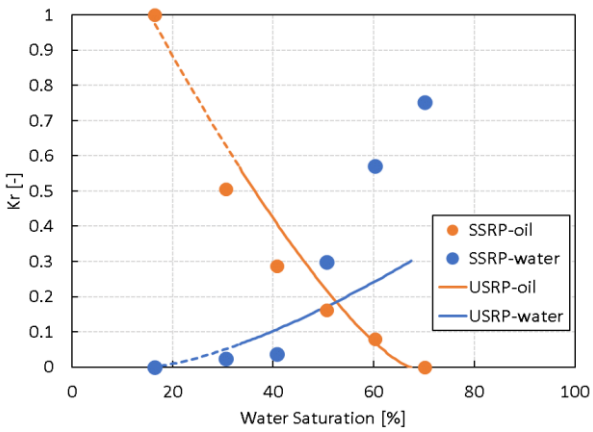

Fig. 14. Steady state relative permeability (SSRP) vs. unsteady state relative permeability (USRP) of fracture sample. Dash line and solid line represents the measurements before and after water breakthrough, respectively.

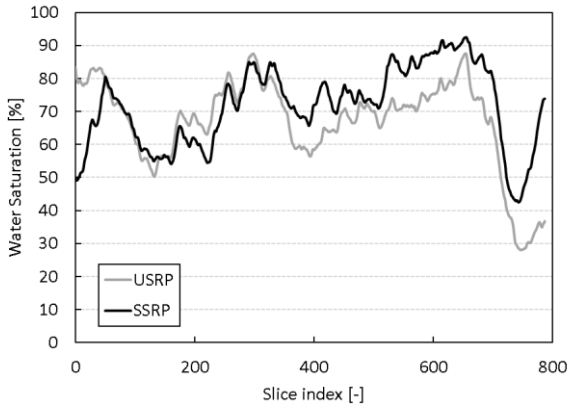

Fig. 15. Water saturation profile of 500^3 voxels subset of Berea sandstone at residual saturation of steady state relative permeability (SSRP) and unsteady state relative permeability (USRP).

3.3 Clay-rich shale

The clay-rich shale sample presents a markedly different form of heterogeneity compared to the fractured sample, primarily due to its fine-grained nature and complex nanoscale pore structure. The screening procedure began with an evaluation of the spatial distribution of connected porosity, as shown in Figure 16. The normalized resolved porosity values were computed as 0.49, 0.46, and 0.52 in the x-, y-, and z-directions, respectively. All values are well below the threshold of 0.9, indicating that porosity is relatively uniformly distributed throughout the scanned volume. This initial result suggests that, despite the inherent heterogeneity of clay-rich media, the porosity itself does not exhibit significant directional bias or large-scale variation within the sampled domain. This can be attributed to the pervasive fine-scale lamination and microstructural consistency of clay-rich systems, in contrast to the abrupt discontinuities seen in fractured rocks.

Pore size distribution analysis further informs the degree of structural representativeness within the scanned volume. As shown in Figure 17, the pore size distribution displays noticeable deviation at small subset volumes but becomes increasingly stable as volume increases, eventually reaching convergence at the full scanned domain. This behavior reflects the characteristic structural uniformity at larger scales, even though individual subsets may contain microstructural variability. The space-filling analysis presented in Figure 18 confirms this: while eight equivalent subvolumes demonstrate minor differences in distribution shape, they all share a similar range of pore sizes. This implies that although local heterogeneities exist, the overall pore size spectrum is consistently captured across the sample. However, the permeability coefficient of variation (COV), shown in Figure 19, is calculated to be 47.2% across the full volume—indicating a moderate level of statistical uncertainty in the permeability field. This level of variability, though lower than that of the fractured sample, still suggests that the flow pathways in the shale are non-uniform and that transport behavior may not be fully captured by a single subvolume.

Multiphase flow simulations were carried out on the full shale volume to compare steady-state relative permeability (SSRP) and unsteady-state relative permeability (USRP), as presented in Figure 20. The results show that USRP of the oil phase agrees well with SSRP across the saturation range. However, SSRP of the water phase is observed to be slightly lower than its USRP counterpart. This discrepancy may be attributed to preferential water flow along micro-laminations or clay-coated pore surfaces that become more accessible during dynamic displacement. Importantly, the residual water saturation profiles shown in Figure 21 display consistent spatial distribution patterns between SSRP and USRP. This agreement in final saturation states supports the observation that, while the clay-rich shale may not strictly satisfy the criteria for a representative elementary volume (REV) due to its moderate COV, it does exhibit a degree of representative behavior sufficient to allow meaningful multiphase flow interpretation at the scale of the current simulation volume.

The clay-rich shale sample does not strictly meet the REV criteria as defined by the screening metrics applied in this study. Nevertheless, the uniform porosity, converging pore size distribution, and partial consistency in flow behavior suggest that it operates within a transitional regime: not fully representative in the strict statistical sense, yet still capable of supporting coherent and physically interpretable flow simulation results. This highlights the unique challenge posed by fine-grained heterogeneous media, where nanoscale pore connectivity, rather than bulk porosity variation, governs fluid displacement behavior.

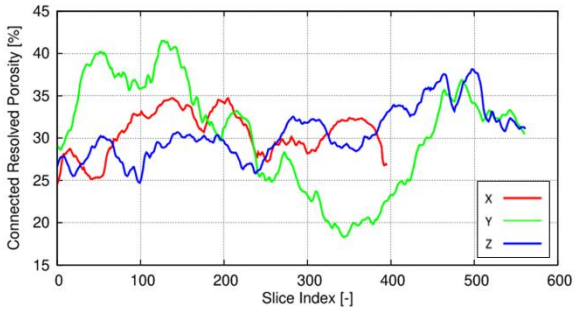

Fig. 16. Connected resolved porosity profiles of clay-rich shale.

Table 3. Normalized resolved porosity ($\emptyset^*$) of clay-rich shale.

X	Y	Z
0.49	0.46	0.52

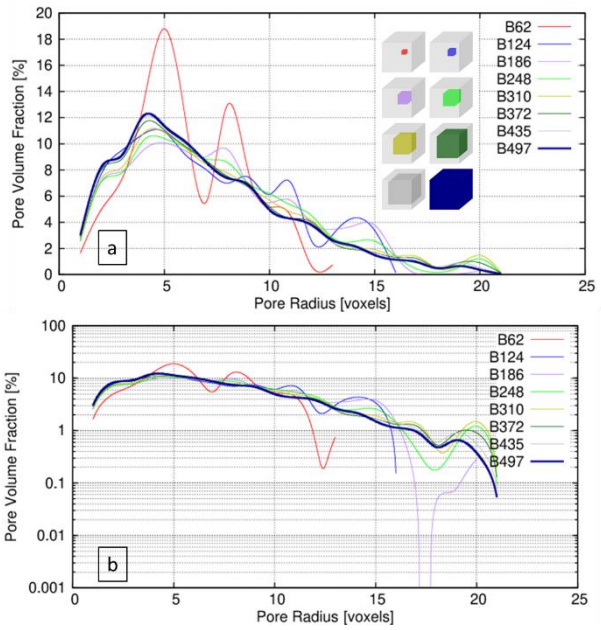

Fig. 17. Size growing analysis of pore size distribution of clay-rich shale in (a) linear scale and (b) logarithmic scale.

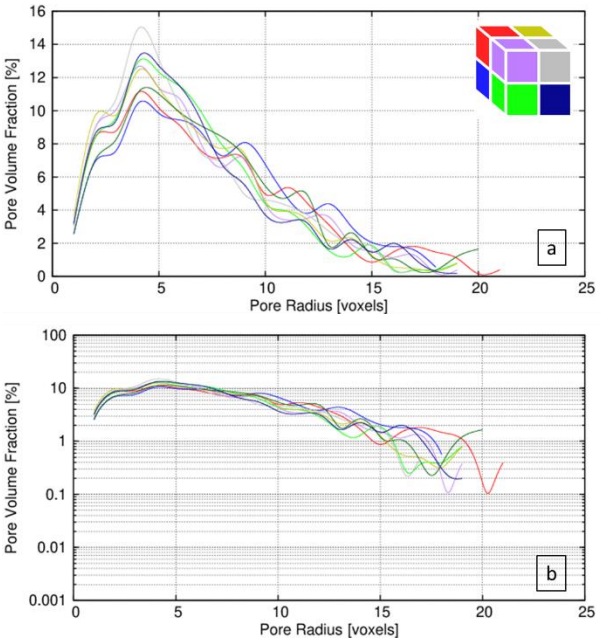

Fig. 18. Space filing analysis of pore size distribution of clay-rich shale in (a) linear scale and (b) logarithmic scale.

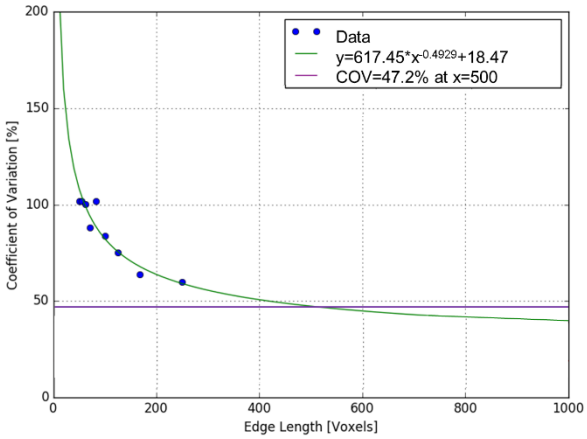

Fig. 19. Permeability coefficient of variance (COV) of clay-rich shale.

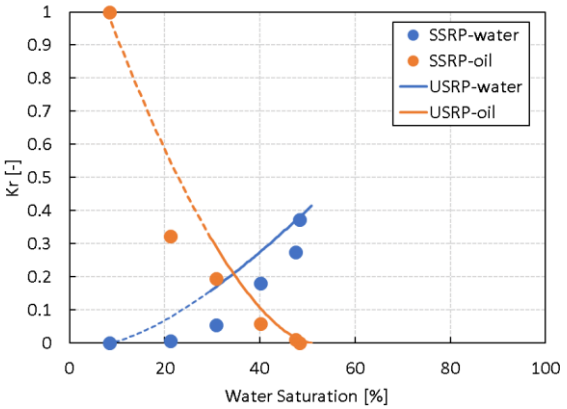

Fig. 20. Steady state relative permeability (SSRP) vs. unsteady state relative permeability (USRP) of clay-rich shale. Dash line and solid line represents the measurements before and after water breakthrough, respectively.

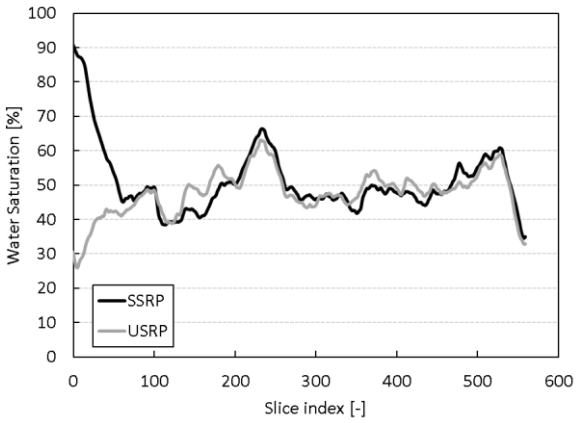

Fig. 21. Water saturation profile of clay-rich shale at residual saturation of steady state relative permeability (SSRP) and unsteady state relative permeability (USRP).

4 Conclusion

This study presents a systematic framework to assess Representative Elementary Volume (REV) and its impact on steady-state and unsteady-state relative permeability

(SSRP and USRP) measurements using high-resolution digital rock imaging and pore-scale simulation. Three samples with varying degrees of heterogeneity, Berea sandstone (homogeneous), a fractured rock (highly heterogeneous), and a clay-rich shale (heterogeneous but fine-grained), were examined through a structured screening procedure. This procedure evaluated porosity uniformity, pore size distribution convergence, spatial variability across subvolumes, and permeability coefficient of variation (COV), establishing clear thresholds for REV assessment.

For the Berea sandstone, low normalized porosity variation and a COV below 20% confirmed the presence of a representative volume (500^3 voxels), where SSRP and USRP results showed strong agreement. In contrast, the fractured sample exhibited non-convergent pore structures, large variability across subvolumes, and a high COV (>75%), indicating the absence of a REV. As a result, significant discrepancies were observed between SSRP and USRP outcomes. The clay-rich shale showed limited porosity variation and convergence in pore characteristics but a moderate COV (~47%), placing it in a transitional zone, non-REV by strict definition, yet capable of producing consistent relative permeability trends.

The uniqueness of this study lies in its integration of a quantitative REV screening protocol with direct comparison of SSRP and USRP behaviors across varying rock types. This combined approach not only clarifies the influence of REV on multiphase flow simulation reliability but also provides a practical, scalable methodology for identifying representative volumes in digital rock workflows. These findings highlight the need to rigorously evaluate representativeness before interpreting flow properties, especially in heterogeneous media, and offer a foundation for more robust pore-to-core scale modeling in future studies.

References

1. M.J. Blunt, Multiphase Flow in Permeable Media: A Pore-Scale Perspective (Cambridge University Press, 2017)
2. N.R. Morrow, N. Mungan, J. Can. Pet. Technol. 4(04), 44 (1965)
3. S. Masalmeh, K. Al-Fossail, A. Al-Kharusi, SPE Reserv. Eval. Eng. 10(04), 326 (2007)
4. S. Akin, A.R. Kovscek, SPE J. 8(04), 410 (2003)
5. J. Bear, Dynamics of Fluids in Porous Media (Dover Publications, 1972)
6. K. Nordahl, P.S. Ringrose, Math. Geosci. 40, 753 (2008)
7. X. Shan, H. Chen, Phys. Rev. E 47(3), 181 (1993)
8. B. Crouse, D.M. Freed, N. et al., SCA 2016-058, Int. Symp. Soc. Core Analysts, Snowmass, CO, USA (2016)
9. G.R. Jerauld, J. Fredrich, N. Lane, Q. Sheng, B. Crouse, D.M. Freed, R. Xu, in SPE Abu Dhabi Int. Pet. Exhib. Conf., Soc. Pet. Eng. (2017)
10. H. Otomo, H. Fan, Y. Li, M. Dressler, I. Staroselsky, R. Zhang, H. Chen, J. Comput. Sci. 17, 334 (2016)
11. H. Chen, C. Teixeira, K. Molvig, Int. J. Mod. Phys. C 9(08), 1281 (1998)
12. X. Shan, X.F. Yuan, H. Chen, J. Fluid Mech. 550, 413 (2006)
13. H. Otomo, B. Crouse, M. Dressler, D.M. Freed, I. Staroselsky, R. Zhang, H. Chen, Comput. Fluids 172, 674 (2018)
14. H. Andrä, N. Combaret, J. Dvorkin, E. Glatt, J. Han, M. Kabel et al., Comput. Geosci. 17(5), 943 (2013).
15. K. Nordahl, P. Ringrose, Math. Geosci. 40, 753 (2008).
16. P. Renard, G. de Marsily, Adv. Water Resour. 20(5–6), 253 (1997).
17. D. Zhang, R. Zhang, S. Chen, W.E. Soll, Geophys. Res. Lett. 27(8), 1195 (2000)
18. R. Hilfer, Adv. Chem. Phys. 92, 299 (1996)
19. G. Sun, Z. Sun, A. Fager, B. Crouse, E3S Web Conf. 367, 01011 (2023)
20. G. Sun, R. Salazar-Tio, J. Yang, H. Otomo, G. Balasubramanian, A. Islam, A. Fager, B. Crouse, R. Zhang, J. Schembre-McCabe, 2023-046, presented at the SCA 2023 Annual Symposium, Society of Core Analysts, Abu Dhabi, UAE (2023)